

DISPATCH: Disarming Adversarial Patches in Object Detection with Diffusion Models

Jin Ma, Mohammed Aldeen, Christopher Salas, Feng Luo, Mashrur Chowdhury, Mert Pesé, Long Cheng
Clemson University

Abstract—Object detection is fundamental to various real-world applications, such as security monitoring and surveillance video analysis. Despite their advancements, state-of-the-art object detectors are still vulnerable to adversarial patch attacks, which can be easily applied to real-world objects to either conceal actual items or create non-existent ones, leading to severe consequences. Given the current diversity of adversarial patch attacks and potential unknown threats, an ideal defense method should be *effective*, *generalizable*, and *robust* against adaptive attacks. In this work, we introduce DISPATCH, the first diffusion-based defense framework for object detection. Unlike previous works that aim to “detect and remove” adversarial patches, DISPATCH adopts a “regenerate and rectify” strategy, leveraging generative models to disarm attack effects while preserving the integrity of the input image. Specifically, we utilize the in-distribution generative power of diffusion models to regenerate the entire image, aligning it with benign data. A rectification process is then employed to identify and replace adversarial regions with their regenerated benign counterparts. DISPATCH is attack-agnostic and requires no prior knowledge of the existing patches. Extensive experiments across multiple detectors and attacks demonstrate that DISPATCH consistently outperforms state-of-the-art defenses on both hiding attacks and creating attacks, achieving the best overall mAP.5 score of 89.3% on hiding attacks, and lowering the attack success rate to 24.8% on untargeted creating attacks. Moreover, it maintains strong robustness against adaptive attacks, making it a practical and reliable defense for object detection systems.

Index Terms—Adversarial patch attacks, Object detection, Diffusion models, Defense

1. Introduction

Object detection stands as a cornerstone in computer vision, serving as the foundation for a wide range of applications such as surveillance systems [1], robotics [2], autonomous driving [3], and augmented reality [4]. It allows AI systems to recognize and locate objects in their surroundings. Modern machine learning-based object detection frameworks, such as YOLO [5], Faster R-CNN [6], and DETR [7], have achieved remarkable detection accuracy and efficiency, making them broadly applied to real-world AI systems. Despite their impressive performance, object

detectors are vulnerable to adversarial attacks [8], [9], which exploit the inherent weaknesses of machine learning models to mislead them into producing incorrect output. Among various adversarial attack strategies, adversarial patch attacks have attracted significant attention from the security community, as they are easy to implement in the real world, and cause severe consequences in object detection systems [9], [10]. In adversarial patch attacks, the adversary creates patches that can be placed on real-world objects, such that when viewed by a machine learning model, these patches trick the model into making incorrect predictions [11]–[15], leading to *hiding attacks* or *creating attacks*. In hiding attacks [12]–[16], the patch is applied to a victim object, making the object invisible to the detection system. For instance, in surveillance systems deployed in sensitive areas such as airports or government buildings, an adversarial patch affixed to clothing can prevent security cameras from recognizing prohibited individuals. In contrast, creating attacks [17]–[19] involves tricking the system into identifying a non-existent object. For example, an adversarial patch could be used to make the surveillance system treat it as a suspect vehicle, leading to unnecessary investigations or divert attention from genuine security events.

In response to the threat of adversarial patch attacks, numerous defense mechanisms have been proposed, either during the model training or inference stage [20]. Training-level defenses focus on retraining the model on adversarial examples or designing a more robust architecture. However, these methods require additional training time and may not be able to defend against unseen attacks. On the other hand, inference-level defenses focus on pre-processing data before the model inference, without the time-consuming model retraining stage. Some existing works for inference-level defense aim to identify images that contain adversarial patches, and then reject them for further processing [21], [22]. While others aim to fix the input images such that detectors can make correct predictions no matter with or without adversarial patches [23], [24]. In this paper, we focus on the latter one since it will not interrupt the input data flow. Given the diversity of existing attacks and potential unforeseen risks in the wild, an ideal defense method should be: **effective** in ensuring the performance of protected detectors, **generalizable** for handling different types of attacks, and **robust** against further adaptive attacks. In this paper, we aim to develop a method that can strike the balance among these requirements.

Object detectors are generally trained to obtain optimal performance on specific datasets, while adversarial patch attacks try to find the patch that cannot be handled by the victim detector, or in other words, the non-robust data or out-of-distribution data for the victim detectors [25], [26]. Previous defense works typically adopt a “detect and remove” strategy, where adversarial patches are first identified using specially designed methods or models, and then removed from the input image. However, such approaches carry the risk of mistakenly removing benign regions, potentially degrading the detection performance. In contrast, our approach is motivated by the goal of “disarming” adversarial patches, transforming them into benign content for the detector, while preserving the overall integrity of the input image. Specifically, Diffusion Models (DMs), as powerful generative models, are trained to learn a generative process that captures the underlying training data distribution, enabling the data generation to be consistent with the original training dataset. That is to say, the outputs of DMs naturally align with the distribution of clean training data.

By leveraging this in-distribution generative power of DMs, we propose DISPATCH to fix the input data, disarming the potential adversarial patches. DISPATCH encompasses a two-stage process: *regeneration stage* and *rectification stage*. In the regeneration stage, DISPATCH employs inpainting diffusion models [27], [28] to regenerate the whole image. The properties of the diffusion process ensure that the regenerated image closely aligns with the benign data distribution. In the rectification stage, DISPATCH employs an adversarial detection algorithm to identify and replace potential adversarial regions with their benign counterparts, leaving clean regions untouched. DISPATCH does not rely on any prior knowledge of existing adversarial patches or the training of specific models. The only requirement is that the Diffusion Model is trained on clean dataset, such that it can generate the in-distribution data for the detector. The main contributions of this paper are as follows:

- 1) **An attack-agnostic and generalizable defense algorithm:** We propose a novel diffusion-based defense method, which disarms adversarial patches for object detectors (called DISPATCH) ¹. Our approach leverages DMs to rectify input images without requiring any prior knowledge of adversarial patch patterns. This makes DISPATCH a generalizable method for defending against diverse adversarial patch attacks.
- 2) **Unique “regenerate and rectify” approach:** Unlike most previous works that focus on “detect and remove” strategies for adversarial patches, DISPATCH introduces a novel “regenerate and rectify” pipeline. This strategy disarms adversarial patches by neutralizing them into benign content through in-distribution generation, rather than explicitly removing them. As a result, it avoids unnecessary alteration of benign regions and preserves the overall integrity of the input image.

1. The source code is available at <https://github.com/MaJinWakeUp/D3>

- 3) **Enhanced defense performance and robustness:** Extensive experiments demonstrate that DISPATCH achieves state-of-the-art performance across different detectors and attacks. It achieves the highest mAP.5 under hiding attacks, and the greatest reduction of attack success rates for creating attacks, consistently outperforms other baselines. Moreover, DISPATCH shows strong robustness against adaptive attacks, showing its resilience under stronger and more targeted threat scenarios.

2. Related Work

2.1. Adversarial Patch Attacks

Adversarial patch attacks pose a significant threat to object detection systems. Current patch attacks can be categorized into creating attacks and hiding attacks. When crafting creating attacks, a commonly used approach is the Expectation over Transformation (EOT) technique, which optimizes a patch with random transformations [29], [30]. For hiding attacks, Thys *et al.* introduced printable adversarial patches that are capable of concealing individuals from object detectors [12]. These patches are easily noticeable to human observers, limiting their stealthiness. To address this limitation, researchers have explored various strategies to enhance the naturalness of adversarial patches. For instance, Huang *et al.* introduced patches with camouflage patterns by incorporating constraints during optimization [31]. Hu *et al.* deployed Generative Adversarial Networks (GANs) to generate patches that feature common imagery, such as animals, making them appear less suspicious [13]. Other approaches focus on utilizing real-world objects with specifically designed textures to evade detection. For example, the authors in [14] developed adversarial textures that can be applied to clothing in arbitrary shapes, enabling individuals wearing such clothes to avoid detection from different viewing angles. More recently, Zhu *et al.* proposed a novel adversarial camouflage texture using 3D modeling techniques, mimicking real-world camouflage patterns to achieve a high degree of naturalness [15]. These advanced and natural-looking attacks expose serious weaknesses in object detectors, highlighting the urgent need for more adaptable defenses.

2.2. Defenses against Adversarial Patch Attacks

Current operation-level defense methods include two approaches: identifying and rejecting images that contain adversarial patches, or fixing input images such that detectors can make correct predictions. Xiang *et al.* developed an objectness predictor and objectness explainer to detect unexplained objectness caused by the adversarial patches, and to trigger an attack alert when such anomalies occur [21]. Feng *et al.* trained two defensive patches, canary and woodpecker, to probe potential adversarial patches [22]. These approaches only raise an alert when adversarial patches

exist, but cannot help detectors make correct predictions under these attacks, limiting their practical applications. Recent works have focused more on fixing the data without interrupting the input data flow. For example, Xiang *et al.* introduced a patch-agnostic masking strategy that removes adversarial patches without prior knowledge of their shape, size, or location [23]. While effective within specific threat models, this approach is limited to scenarios involving only a single adversarial patch per image. Liu *et al.* developed a patch segmentation model to identify adversarial patches, followed by a shape-completion step to refine detection and remove the patches from images [32]. Tarchoun *et al.* identified adversarial patches by detecting entropy peaks in the image and used an autoencoder to inpaint the affected areas [33]. Jing *et al.* utilized semantic independence and spatial heterogeneity, supported by the Segment-Anything-Model (SAM), to effectively localize patches [34]. Lin *et al.* proposed a block-based method in which an autoencoder was used to detect adversarial regions by rejecting out-of-distribution blocks [24]. Our DISPATCH differs from previous works in two aspects. First, instead of following the conventional “detect and remove” paradigm, which risks over-removing benign regions, we adopt a “regenerate and rectify” strategy. This approach disarms adversarial patches by transforming them into in-distribution content, thereby preserving the integrity of the input image. Second, DISPATCH does not require training any attack-specific models. It operates directly on off-the-shelf diffusion models, and achieves remarkable performance compared to prior methods that rely on customized or trained defense networks.

3. Preliminary

3.1. Diffusion Models

Diffusion models (DMs) usually comprise three main components: the forward process, the reverse process, and the sampling procedure [35]. The forward process incrementally adds noise to the input data, effectively transforming it into a noise distribution. In contrast, the reverse process attempts to reconstruct the original data distribution $p(x)$ by learning to iteratively denoise the noisy samples. The sampling procedure leverages the trained reverse process to generate new data points by starting from a random noise and progressively refining it.

In the field of image synthesis, Denoising Diffusion Probabilistic Models (DDPM) have emerged as one of the most successful and widely adopted approaches [36], [37]. They can be interpreted as a sequence of denoising autoencoders $z_\theta(x_t; t)$, indexed by time steps $t = 1, \dots, T$. Here, $z_\theta(x_t; t)$ represents the autoencoder’s prediction of the noise added to the input x_t , which is a progressively degraded version of the original data x , with θ denoting the parameters of the model. At each step, the autoencoder takes a noisy input x_t and predicts the noise added during the forward diffusion process. The objective is to iteratively refine x_t by subtracting the predicted noise to recover the original data distribution. The training objective of DDPMs

is to minimize the distance between the real noise z_t (the actual noise added at time step t during the forward diffusion process) and the model’s predicted noise $z_\theta(x_t; t)$, which can be represented as:

$$L_{DM} = \mathbb{E}_{x, z \sim \mathcal{N}(0,1), t} \| z_t - z_\theta(x_t; t) \|^2 \quad (1)$$

with t uniformly sampled from $\{1, \dots, T\}$.

DMs are also capable of modeling conditional distributions $p(x|y)$, enabling the generative process to be guided by specific conditions y , such as class labels, textual descriptions, or other auxiliary data. These models, referred to as conditional DMs, allow for controlled generation by incorporating the additional conditioning information into the denoising process. In conditional DMs, the denoising model is adjusted to take the conditioning input into account, making the prediction $z_\theta(x_t; t; y)$, where y provides the conditioning context. The training objective for conditional DMs is an extension of the original DDPM objective and is formulated as:

$$L_{CDM} = \mathbb{E}_{x, y, z \sim \mathcal{N}(0,1), t} \| z_t - z_\theta(x_t; t; y) \|^2 \quad (2)$$

This objective ensures that the model learns to denoise while incorporating the conditioning information y , which enables accurate and controlled synthesis conditioned on the provided context.

Denoising Diffusion Implicit Models (DDIMs) [38] offer a more efficient alternative to DDPMs by allowing fewer sampling steps without compromising the output quality. DDIMs achieve this by modifying the reverse process, enabling faster sampling while maintaining high fidelity in the generated data. The trade-off between sampling speed and output quality in DDIMs makes them suitable for applications requiring real-time generation.

3.2. Diffusion for OOD Detection

In this work, we address adversarial patch defense by leveraging the observation that adversarially perturbed data diverges from the distribution of clean data, which has been explored in previous adversarial detection research [24], [39]. While prior studies often treat this as an out-of-distribution (OOD) detection problem, our approach goes a step further: rather than merely detecting OOD regions, we aim to transform them back into in-distribution content. DMs are particularly well-suited for this task due to their generative capacity to model and reproduce the underlying data distribution. Prior work [40] has applied inpainting DMs for image-level OOD detection by comparing generated image with original image. However, this method stops at image-level OOD detection. In this paper, we extend the application of DMs to rectify adversarial patches at the pixel level. Our proposed method, DISPATCH, leverages inpainting DMs to regenerate the entire image without any prior knowledge of the adversarial patches. We then identify inconsistencies between the original and regenerated images to locate adversarial regions, which are subsequently replaced by their benign, in-distribution counterparts.

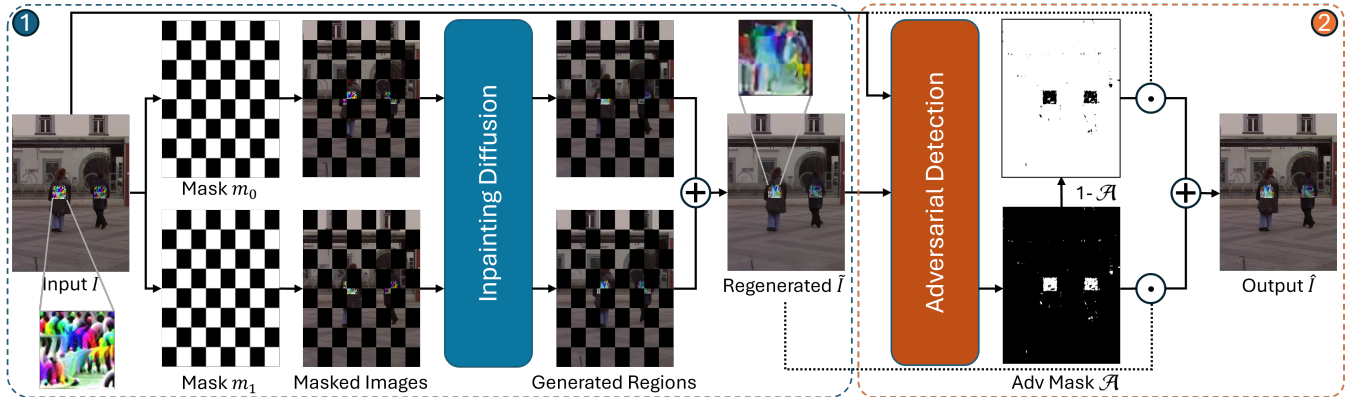


Figure 1: The DISPATCH pipeline consists of two key stages ① The regeneration stage, which generates a fully reconstructed image to disarm adversarial patches. ② The rectification stage, which replaces adversarial regions in the input image with generated benign counterparts, according to the adversarial mask predicted by our adversarial detection algorithm.

4. The Proposed Method

4.1. Threat Model

We assume the adversary aims to deceive victim object detectors by introducing adversarial patches into input images. These patches can either be digitally added directly to the image or physically applied to real-world objects, impacting the images captured by cameras. The adversary has the flexibility to modify the size, shape, and location of the patches to achieve one of two objectives: Hiding Attack (HA), where existing objects are concealed, or Creating Attack (CA), where non-existent objects are fabricated. A critical constraint is that the *adversarial patch should not fully occlude the object*, as complete occlusion renders the object unrecoverable, even by a human expert. We assume a strong adversary with full knowledge of the object detector’s architecture and weights, enabling a white-box attack. Additionally, the adversary is aware of the defense method, DISPATCH, and can design adaptive attacks accordingly. However, the adversary is not permitted to tamper with or modify the object detector or the defense model itself.

4.2. Overview of DISPATCH

Figure 1 illustrates the DISPATCH pipeline, which comprises two key stages: ① regeneration stage and ② rectification stage. In the regeneration stage, the entire input image is regenerated through an inpainting diffusion model, using two unique inpainting masks. The goal in this stage is to produce a reconstructed image containing only in-distribution data, effectively removing any adversarial artifacts. However, the regenerated image cannot be directly used for detection, since the benign objects may be affected during the regeneration process (Appendix A.1). *We aim to only replace the possible adversarial regions with the regenerated counterparts, while keeping the others in their original form.* In the rectification stage, the regenerated image is compared with the original input image to identify

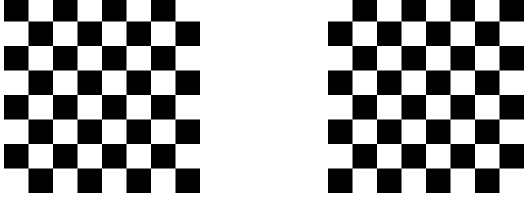
potential adversarial regions by using an effective adversarial detection algorithm, described in Section 4.4. After obtaining the adversarial mask \mathcal{A} , the suspected regions in the original input are replaced with the corresponding content from the regenerated image. This two-stage process ensures that the final output is both free of adversarial influences and retains the integrity of clean regions.

4.3. Regeneration Stage

To regenerate the entire image efficiently and ensure it contains only benign in-distribution pixels, we use an off-the-shelf inpainting diffusion model to perform this task. The inpainting diffusion model takes as input the original image and a mask specifying regions for inpainting, generating new content in the masked areas based on contextual information from the unmasked regions, as shown in Figure 1. However, since the inpainting process relies on the unmasked regions for context, only a partial image can be regenerated in each forward pass. This leads to a key challenge: *“How can we regenerate the entire image with the minimum number of forward passes while preserving its original content?”*

Efficient regeneration strategy. We use two complementary binary masks: the checkerboard mask m_0 and its inverse checkerboard mask m_1 , as shown in Figure 2. These masks, previously used for image-level OOD detection [40], are repurposed here for image regeneration. Each mask consists of $N \times N$ grids, where a value of 1 (white) indicates the region to be regenerated, and 0 (black) represents the preserved region. Since $m_0 \oplus m_1 = J$, where \oplus is an element-wise summation, J is a matrix full of ones, the combination of these two masks ensures that all regions of the input image are regenerated across two inpainting passes, and the unmasked areas in each pass provide sufficient contextual information for accurate inpainting.

Regeneration process. Given an input image I , and two masks m_0 and m_1 , we process the image in parallel through



(a) Checkerboard mask m_0 (b) Inverse checkerboard mask m_1

Figure 2: Example of the checkerboard mask and its inverse mask with 8×8 grids. These masks are used in inpainting DMs to regenerate all regions within an input image.

the inpainting diffusion model \mathcal{D} , generating two inpainted images \tilde{I}_0 and \tilde{I}_1 :

$$\tilde{I}_0 = \mathcal{D}(I; m_0), \quad \tilde{I}_1 = \mathcal{D}(I; m_1) \quad (3)$$

The final fully regenerated image \tilde{I} is obtained by combining the inpainted regions from \tilde{I}_0 and \tilde{I}_1 according to their respective masks:

$$\tilde{I} = \tilde{I}_0 \odot m_0 \oplus \tilde{I}_1 \odot m_1 \quad (4)$$

Here, \odot denotes element-wise multiplication. By using this efficient masking strategy, we ensure that the entire image is regenerated with only two forward passes of the diffusion inpainting model, minimizing computational overhead while maintaining high-quality in-distribution reconstruction. Since the entire image is processed in this stage, adversarial patches, regardless of their location or shape, are effectively transformed into benign, in-distribution data.

4.4. Rectification Stage

In this stage, we aim to find the potential adversarial regions and replace them with the corresponding regenerated content, while keeping the benign regions in their original form. Given the properties of the diffusion network, the regenerated image \tilde{I} is inherently an in-distribution image. As a result, regions affected by adversarial patches, when regenerated, tend to exhibit a different distribution from their original adversarial form. As illustrated in Figure 1, the adversarial patch in \tilde{I} differs significantly from the corresponding patch in I . Conversely, the regenerated content within benign regions should closely align with the distribution of the original benign pixels. Leveraging this characteristic, we propose an effective adversarial detection approach to identify potential adversarial regions.

Adversarial detection. The proposed adversarial detection algorithm is shown in Algorithm 1. We first normalize both the original image $I \in \mathbb{R}^{3 \times W \times H}$ and the regenerated image $\tilde{I} \in \mathbb{R}^{3 \times W \times H}$ to the range of $[0, 1]$, where 3 is the RGB channels, W and H are the sizes of the image (Line 1 in Algorithm 1). Then, we compute the pixel-wise L2 distance matrix $D \in \mathbb{R}^{W \times H}$, where each element in D is computed as:

$$D[i, j] = \|I[i, j] - \tilde{I}[i, j]\|_2, \quad 1 \leq i \leq W, 1 \leq j \leq H \quad (5)$$

Algorithm 1: Adversarial Detection Algorithm

Input: $I \in \mathbb{R}^{3 \times W \times H}$, $\tilde{I} \in \mathbb{R}^{3 \times W \times H}$

Output: Adversarial mask $\mathcal{A} \in \mathbb{R}^{W \times H}$

- 1 Normalize I and \tilde{I} to $[0, 1]$;
 - 2 Compute distance matrix

$$D[i, j] = \|I[i, j] - \tilde{I}[i, j]\|_2, \quad \forall i, j;$$
 - 3 Blur D to reduce noise;
 - 4 Flatten D into vector $\mathbf{d} \in \mathbb{R}^{W \cdot H}$;
 - 5 Apply KMeans clustering on \mathbf{d} to obtain clusters ϕ_0 (smaller centroid) and ϕ_1 (larger centroid);
 - 6 **for** $i = 1$ **to** W **do**
 - 7 **for** $j = 1$ **to** H **do**
 - 8 $\mathcal{A}[i, j] \leftarrow 1$ if $D[i, j] \in \phi_1$, else $\mathcal{A}[i, j] \leftarrow 0$;
 - 9 **end**
 - 10 **end**
 - 11 **return** \mathcal{A}
-

$I[i, j]$ and $\tilde{I}[i, j]$ represent the RGB vectors at pixel (i, j) . To mitigate noise introduced by the stochastic nature of image generation, the distance matrix D is subsequently blurred using a smoothing filter. This blurring operation helps to reduce local fluctuations and smooth adjacent areas.

We then use the distance matrix D to identify adversarial regions and benign regions, based on the observation that adversarial regions typically exhibit larger distance values. We flatten the distance matrix into a vector $\mathbf{d} \in \mathbb{R}^{W \cdot H}$, and apply KMeans clustering [41] with $k = 2$. This operation yields two clusters: ϕ_0 and ϕ_1 , where ϕ_0 corresponds to the cluster with a lower centroid value (benign regions), and ϕ_1 corresponds to the cluster with a higher centroid value (potential adversarial regions). Pixels belonging to ϕ_1 are thus marked as adversarial in the mask \mathcal{A} :

$$\mathcal{A}[i, j] = \begin{cases} 0 & : D[i, j] \in \phi_0 \\ 1 & : D[i, j] \in \phi_1 \end{cases}, \quad 1 \leq i \leq W, 1 \leq j \leq H \quad (6)$$

Final output. According to the adversarial mask \mathcal{A} predicted by Algorithm 1, we combine I and \tilde{I} to obtain the final output:

$$\hat{I} = \mathcal{A} \odot \tilde{I} \oplus (1 - \mathcal{A}) \odot I \quad (7)$$

In this step, those potential adversarial pixels identified by \mathcal{A} are replaced with their generated counterparts in \tilde{I} , while the remaining pixels retain their original values from the input image I .

This approach enables the proposed algorithm to efficiently identify adversarial regions within an image by leveraging the differences between the original input and the regenerated image. The clustering step automatically segments pixels into adversarial and benign categories, eliminating the need for prior thresholding or manual intervention. It is worth mentioning that even if some benign regions are mistakenly identified as adversarial, the rectification process does not degrade their quality. This resilience comes from the design of DISPATCH, which replaces suspect regions

rather than removing them entirely. As a result, the overall visual fidelity of benign regions is preserved after processing. We show the accuracy of this adversarial detection algorithm in Appendix A.2.

4.5. Diffusion Networks

To reduce the time complexity of the regeneration stage in DISPATCH, we adopt the Latent Diffusion Model (LDM) [28] as the backbone for inpainting. LDM operates in a latent space, where autoencoders process a compressed representation of the image instead of working directly in the image space. This design significantly improves the efficiency of the generation process while maintaining high-quality reconstructions, making LDM an ideal choice for DISPATCH. We employ the LDM with a DDIM sampler, and resize the images to 512×512 for the inpainting. Notably, we use the original pretrained inpainting LDM weights provided by the authors, which are trained on MS-COCO dataset [42], without any additional fine-tuning.

5. Experiments

In this section, we evaluate DISPATCH on existing benchmarks and real-world scenarios under various types of patch attacks, and compare its performance with other SOTA defense methods, including a certifiable defense method ObjectSeeker (OS) [23], and four empirical defense methods SAC [32], Jedi [33], PAD [34], and NutNet [24]. Given the inherent randomness of diffusion models, all results for the proposed DISPATCH are reported as the average of three runs. The default number of grids is set to $N = 32$, and the default sampling steps of LDM is set to $s = 5$ in our experiments. Due to page limitation, we present the results of the ablation study for these two parameters in Appendix A.3 and A.4, respectively. All experiments were performed on a server with an NVIDIA A100 GPU.

5.1. Evaluation on Digital Hiding Attacks

Dataset. In this section, we evaluate DISPATCH on the INRIA-Person [43] dataset for defending against digital hiding attacks. INRIA-Person has been widely used for person detection tasks, it includes 614 images for training and 288 images for testing, where each image contains at least one person. This dataset has been utilized in previous studies for developing various attack methods on person detectors [12], [13], [15], and for assessing defense methods against these attacks [24], [33], [34].

Victim object detectors. To ensure fair evaluation across a diversity of attack methods, we select three victim detectors: YOLOv3 [5], Faster RCNN [6], and DETR [7]. YOLOv3 and Faster RCNN are two representative CNN-based object detectors, with YOLOv3 representing single-stage detectors and Faster RCNN representing two-stage detectors. DETR, in contrast, is a Transformer-based object detector. In our experiment, we implement these detectors

using the MMDetection toolbox [44] and utilize pretrained models on the MS-COCO [42] dataset.

Attack methods. Person-hiding attacks have been extensively studied due to their diverse real-world manifestations and significant security implications. In our experiments, we select three representative attack methods: adversarial patch attack (AdvPatch) [12], naturalistic patch attack (NatPatch) [13], and adversarial texture attack (AdvTexture) [14]. These methods vary in form and attack capability. To ensure consistency, we retrain these attack methods on the training split data, targeting the three victim object detectors. Then we apply the trained patches to the testing data for evaluation. The adversarial patch is applied to every person within one test image. For AdvPatch and NatPatch, we set the patch size to 0.2, following the settings provided in their open-source code [45]. This scale ratio represents the patch height relative to the diagonal length of the victim object bounding box. For AdvTexture, we adjust the scale ratio to 0.25 in our experiments, as it simulates human clothing, which covers more regions of the victim person. We show that DISPATCH is robust to changes in patch size in Appendix A.5. For clarity in our experiments, we use the notation “Detector-Attack” to specify an attack method targeting a particular detector. For example, YOLOv3-AdvPatch indicates implementing AdvPatch attack against YOLOv3 object detector.

Evaluation metrics. We report the mean average precision (mAP) of different detectors for comparison, a widely used metric for evaluating both attack and defense methods [24], [34]. The intersection over union (IoU) threshold for determining a correct prediction is set to 0.5 (mAP.5), which means a detected bounding box is considered correct if its IoU with the ground truth is at least 0.5. In addition, we use the average recall (AR) as a complementary evaluation metric. AR measures the average fraction of ground-truth objects that are successfully detected across different IoU thresholds and object sizes. It provides a comprehensive assessment of a detector’s ability to recover true positives. For both mAP and AR, higher values indicate better defense performance.

Quantitative results. Table 1 shows the quantitative performance of DISPATCH compared to baseline defense methods under various adversarial attacks. For each row, the best defense method is marked in **bold** text, while the second best defense method is marked with an underline. The Clean rows indicate the performance on clean images without any attack, while the Vanilla column represents the results of detectors without any defense applied. We also show the overall performance of each method in the bottom block, on clean images and attacked images. From the Vanilla column, we can observe that all object detectors are vulnerable to three adversarial attacks, where transformer-based DETR is more robust than CNN-based YOLOv3 and Faster RCNN. Regarding defense methods, ObjectSeeker (OS) is a certifiable defense method with a threat model that assumes only a single adversarial patch is present within an image. However, its performance degrades significantly in our experiments, as most images contain

TABLE 1: The performance of DISPATCH compared with other defense methods against hiding attacks on INRIA-Person benchmark. \dagger indicates the certifiable defense method, while the others are empirical defense methods. ObjectSeeker (OS) is not applicable to YOLOv3, so we do not report the results in this table.

Object Detector	Attack	No Defense		With Defense											
		Vanilla		OS \dagger [23]		SAC [32]		Jedi [33]		NutNet [24]		PAD [34]		DISPATCH	
		mAP.5	AR	mAP.5	AR	mAP.5	AR	mAP.5	AR	mAP.5	AR	mAP.5	AR	mAP.5	AR
YOLOv3	Clean	0.910	0.695	-	-	0.900	0.672	0.935	0.668	0.919	0.687	0.909	0.688	0.934	0.680
	AdvPatch [12]	0.498	0.501	-	-	0.579	0.514	0.750	0.558	0.808	0.625	0.811	0.626	0.903	0.649
	NatPatch [13]	0.707	0.593	-	-	0.687	0.562	0.760	0.555	0.746	0.597	0.819	0.633	0.840	0.605
	AdvTexture [14]	0.747	0.618	-	-	0.735	0.592	0.891	0.644	0.811	0.623	0.850	0.657	0.873	0.627
Faster RCNN	Clean	0.963	0.722	0.886	0.650	0.942	0.702	0.953	0.692	0.960	0.713	0.964	0.722	0.965	0.705
	AdvPatch [12]	0.510	0.546	0.184	0.152	0.597	0.557	0.842	0.624	0.852	0.663	0.914	0.692	0.932	0.682
	NatPatch [13]	0.713	0.629	0.274	0.212	0.732	0.620	0.777	0.595	0.750	0.627	0.901	0.683	0.906	0.654
	AdvTexture [14]	0.598	0.657	0.547	0.437	0.574	0.620	0.836	0.660	0.686	0.662	0.888	0.699	0.818	0.662
DETR	Clean	0.945	0.737	0.916	0.668	0.929	0.728	0.939	0.727	0.949	0.740	0.944	0.735	0.954	0.729
	AdvPatch [12]	0.656	0.659	0.410	0.325	0.683	0.633	0.857	0.691	0.861	0.695	0.889	0.718	0.932	0.711
	NatPatch [13]	0.877	0.715	0.782	0.575	0.865	0.692	0.904	0.702	0.899	0.708	0.886	0.712	0.925	0.702
	AdvTexture [14]	0.871	0.722	0.784	0.582	0.857	0.698	0.887	0.701	0.897	0.718	0.891	0.715	0.909	0.715
Overall	Clean	0.939	0.718	0.901	0.659	0.924	0.701	0.942	0.696	0.943	0.713	0.939	0.715	0.951	0.705
	Under Attacks	0.686	0.627	0.497	0.381	0.701	0.610	0.834	0.637	0.812	0.658	0.872	0.681	0.893	0.667

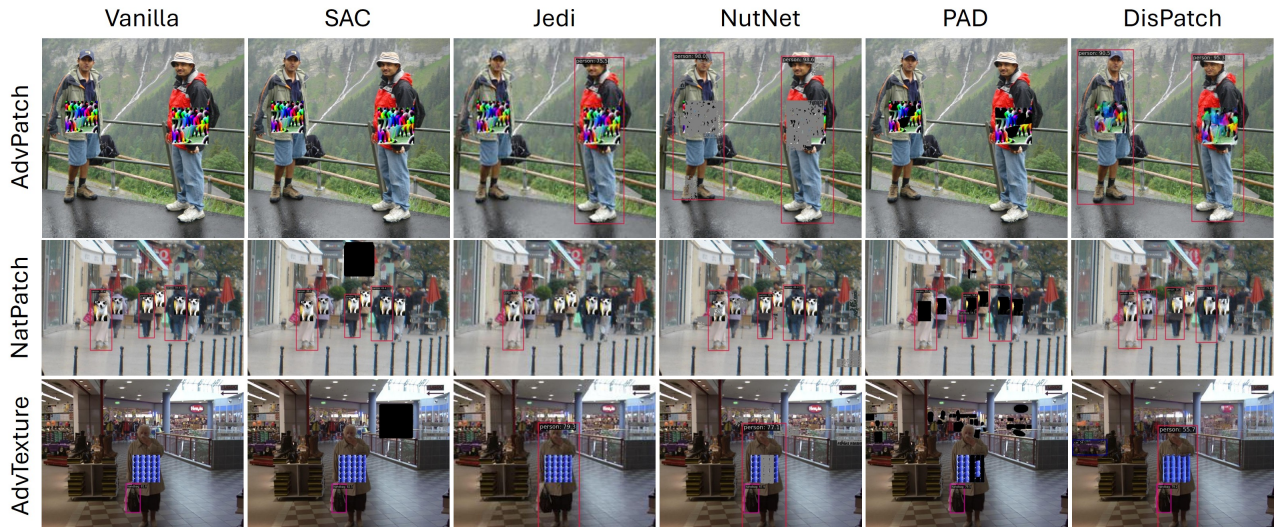


Figure 3: Qualitative results of our DISPATCH compared with other baseline methods when defending YOLOv3 against AdvPatch, NatPatch, and AdvTexture attacks on INRIA-Person dataset. Red bounding boxes indicate the detected persons.

multiple adversarial patches, violating its core threat model assumption. Among the empirical defense methods, SAC can only improve the performance of victim detectors under AdvPatch attack, but lacks generalization to the other two attacks NatPatch and AdvTexture. Jedi, PAD, and NutNet adopt different strategies to detect and mitigate adversarial patches, yielding varying defense results. Jedi and NutNet show similar overall performance, with Jedi performing better on mAP.5, while NutNet performs better in terms of AR. PAD obtains the best performance among all baselines, with a mAP.5 of 0.872 and AR of 0.681. Our method DISPATCH achieves the best overall mAP.5 performance of 0.893, 2.1% better than PAD, and the second best AR of 0.667, 1.4% behind PAD. Although PAD performs well on these hiding attacks, it has significantly higher time complexity compared to DISPATCH, which will be discussed in Section 5.4. For clean images, the proposed DISPATCH achieves even better

mAP.5 score than Vanilla detection results, with a slight drop on AR, which is common in other baselines.

Qualitative results. Figure 3 shows sample results of our DISPATCH method, compared to the other baseline methods, in defending YOLOv3 against AdvPatch, NatPatch, and AdvTexture. Additional results for Faster RCNN and DETR are provided in Appendix B.1. Without any defense (Vanilla), all of the three types of attacks successfully hide at least one person in the demo images. SAC cannot find the actual patches within all demo images. Jedi also fails to identify the adversarial patches, but its aggressive resize operation to 224x224 can help reduce the impact of some patches. NutNet successfully detects adversarial patches in both AdvPatch and AdvTexture examples, but fails to identify the patches in the NatPatch example. PAD removes only a small portion of the adversarial patches in the AdvPatch example and AdvTexture example, leading to

two unsuccessful defenses. But it can detect all patches in NatPatch example. In contrast, our proposed method, DISPATCH, successfully replaces the adversarial patches with benign counterparts, enabling correct detection in AdvPatch and AdvTexture examples. Additionally, in the NatPatch example, DISPATCH recovers one previously undetected person. Although patch-like patterns may still be visually noticeable in the outputs of DISPATCH, these regions no longer retain adversarial functionality.

TAKEAWAY—①: DISPATCH obtains the best overall mAP.5 when facing different person hiding attacks. The only comparable baseline PAD introduces much higher time complexity than DISPATCH. Our unique “regenerate and rectify” approach demonstrates its effectiveness in defending hiding attacks.

5.2. Evaluation on Physical Hiding Attacks

Dataset. To evaluate the proposed method in real-world applications, we printed the AdvPatch trained on the INRIA-Person benchmark, targeting two victim detectors, YOLOv3 and Faster RCNN. We excluded DETR from this evaluation, as it demonstrated inherent robustness in real-world settings. We set the printed patch size to 12×12 inches, and attached it to a person for testing. Multiple videos were recorded in different environmental conditions: indoor, outdoor lighting (Outdoor-L), and outdoor shadow (Outdoor-S). Importantly, personally identifiable information (PII) was removed from these videos. We selected 600 frames in total from these videos to test the performance of victim detectors, with three different defense conditions: no defense (Vanilla), NutNet [24], and DISPATCH.

Results. We use average attack success rate (ASR) as our primary evaluation metric because it is easier to interpret and directly reflects whether an attack hides the target object. Unlike mAP or AR, ASR allows straightforward human verification of success or failure in real world. Given that every individual in our dataset is clearly visible, we expect the detector to assign high confidence scores to such clearly detectable objects. Therefore, we set the confidence score threshold as 0.9 when calculating ASR. An attack is considered successful if no predicted bounding box has both a confidence score above 0.9 and an IoU greater than 0.5 with the ground-truth bounding box of the targeted person. All evaluation results are cross-validated by two co-authors of this paper to ensure accuracy, with a Cohen’s Kappa agreement score of 1. Experimental results are shown in Table 2. The ASRs of AdvPatch are high on the Vanilla detectors, with over 80% on YOLOv3 and over 35% on Faster RCNN. Regardless of the environment, the proposed DISPATCH significantly reduces the ASR to low values, and consistently outperforms the baseline method NutNet. These results demonstrate that DISPATCH can successfully reduce the impact of adversarial patches in real-world scenarios, and improve the predicted confidence scores of victim ob-

TABLE 2: Average Attack Success Rate (ASR) of the AdvPatch attack in real-world tests under three different environmental conditions.

Detectors	YOLOv3			Faster RCNN		
	Vanilla	NutNet	DISPATCH	Vanilla	NutNet	DISPATCH
Indoor	0.99	0.24	0.20	0.42	0.09	0.02
Outdoor-L	0.80	0.23	0.17	0.43	0.13	0.09
Outdoor-S	1.00	0.27	0.26	0.36	0.03	0.00

jects to a high level (beyond 0.9). Some qualitative examples are shown in Appendix B.2.

5.3. Evaluation on Creating Attacks

Dataset. We use an existing benchmark APRICOT [30] to evaluate the defense performance of DISPATCH under creating attacks. APRICOT provides a collection of photos with physical adversarial patches in a variety of real-world scenarios, where the patches are trained to create non-existent objects. The 873 test images in the benchmark were directly used for evaluation, where each image contains one adversarial patch with different shapes. We exclude the ObjectSeeker [23] from the comparison methods in this section, as it is specifically designed to solve hiding attacks.

Victim object detectors. The adversarial patches in APRICOT were trained to attack three different object detectors, Faster RCNN [6], SSD [46], and RetinaNet [47]. In our experiments, we focus on white-box attacks, which means the attacker knows the details of victim object detector. The goal of the attacker is to launch either untargeted or targeted attacks. Untargeted attacks make the detector predict a non-existent object based on the adversarial patch, regardless of the predicted object class, while targeted attacks make the detector predict a specific target class based on the adversarial patch.

Evaluation metrics. We use mAP.5 and attack success rate (ASR) to evaluate the defense performance. When using mAP.5 for evaluation, the adversarial patch is considered as the ground truth. For ASR, we follow the definition in APRICOT [30] and define a successful attack as “at least one bounding box is wrongly predicted by the victim object detector, which has confidence over 0.3 and IoU of 0.1 with the adversarial patch”. The ASR measures the proportion of adversarial examples where the attack successfully deceives the detector. Note that for the creating attack, lower mAP and ASR scores indicate better defense performance.

Quantitative results. Table 3 shows the performance of different defense methods on the APRICOT benchmark. The ASRs of targeted attacks are low on Vanilla detectors, with an overall score of 0.082. The overall ASR of untargeted attacks on Vanilla detectors is 0.424, showing that untargeted attacks work much better than targeted attacks in the real world. These results are consistent with original APRICOT results [30]. Among all the defense baselines, PAD performs the best when defending against targeted attacks, with mAP.5 of 0 and ASR of 0.007 on RetinaNet specifically. On the other hand, NutNet outperforms the other baselines when defending against untargeted attacks, with the lowest

TABLE 3: The mAP.1 and ASR performance of proposed method compared with other defense methods against creating attack on APRICOT dataset. In this table, the lower values indicate better defense performance.

Detector	Metrics	No Defense		Defense									
		Vanilla		SAC [32]		Jedi [33]		NutNet [24]		PAD [34]		DISPATCH	
		mAP.5	ASR	mAP.5	ASR	mAP.5	ASR	mAP.5	ASR	mAP.5	ASR	mAP.5	ASR
Faster RCNN	Targeted	0.123	0.171	0.028	0.037	0.026	0.030	0.051	0.067	0.025	0.037	0.018	0.017
	Untargeted	0.355	0.589	0.164	0.431	0.197	0.415	0.087	0.338	0.158	0.398	0.114	0.327
SSD	Targeted	0.012	0.017	0.013	0.017	0.036	0.049	0.007	0.007	0.005	0.007	0.004	0.003
	Untargeted	0.111	0.315	0.181	0.437	0.064	0.231	0.014	0.178	0.097	0.301	0.015	0.171
RetinaNet	Targeted	0.043	0.059	0.029	0.035	0.013	0.021	0.017	0.024	0.000	0.007	0.009	0.019
	Untargeted	0.156	0.368	0.125	0.365	0.170	0.365	0.050	0.233	0.097	0.316	0.080	0.247
Overall	Targeted	0.059	0.082	0.023	0.030	0.025	0.033	0.025	0.033	0.010	0.017	0.010	0.013
	Untargeted	0.207	0.424	0.157	0.411	0.144	0.337	0.050	0.250	0.117	0.338	0.070	0.248

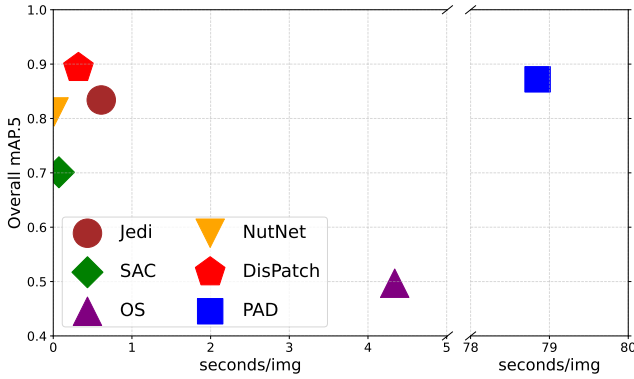


Figure 4: The trade-off figure between efficiency (seconds/img) and effectiveness (Overall mAP.5).

mAP.5 scores on all three detectors. Our method DISPATCH achieves the lowest ASRs on Faster RCNN and SSD when defending against either targeted or untargeted attacks, and the second best performance on RetinaNet. In conclusion, DISPATCH shows the best overall performance when facing targeted attacks, and competitive performance as NutNet when facing untargeted attacks. Note that although PAD has an overall performance similar to DISPATCH for hiding attacks (Table 1), it falls behind DISPATCH in creating attacks, especially untargeted attacks (Table 3). Similarly, although NutNet performs well on creating attacks, it underperforms DISPATCH on hiding attacks. Overall, our proposed method DISPATCH demonstrates consistent superior performance across different types of attacks.

Qualitative Results. We show the qualitative results of DISPATCH, compared to the other baselines, for defending creating attacks in Figure 5. The top-to-bottom rows show attacks on Faster RCNN, SSD, and RetinaNet, respectively. In all three examples, the attacks successfully mislead the detectors into identifying the patches as objects. SAC can only locate and remove the adversarial patch in the RetinaNet example, showing its limited performance. Jedi does not find any adversarial patches in these examples, but its resize operation helps reduce the impact of the adversarial patches, along with some missing (*chair* in SSD example) or incorrect (*stop sign* in RetinaNet example) predictions. NutNet successfully detects all patches in the examples but

also masks out some benign regions. PAD is also capable of identifying all adversarial patches, however, it replaces them with black pixels. These blacked-out regions are still recognized as objects by detectors such as Faster RCNN and SSD, leading to false positive detections. The proposed DISPATCH disarms adversarial patches in all examples with regenerated benign content, showing its effectiveness against these noise-like creating attacks. Upon analyzing these examples, we observe that existing “detect and remove” baselines have the risks of either removing benign regions or failing to eliminate non-existent objects, even after the patches are removed. DISPATCH can reduce these risks through our “regenerate and rectify” approach.

TAKEAWAY—②: DISPATCH reduces the ASR of creating attacks to the lowest level compared to the other baselines. Remarkably, DISPATCH shows consistent effectiveness on both hiding and creating attacks, while other baselines may excel at one type of attack but not the other.

5.4. Time Complexity Analysis

The efficiency of defense algorithms is a critical factor for their deployment in real-world systems. In Figure 4, we present a trade-off between the efficiency and effectiveness of various defense methods against hiding attacks on INRIA-Person. The X-axis represents the average processing time for one input image (excluding the detector processing time), while the Y-axis shows the average mAP.5 across all hiding attacks and detectors. An ideal defense algorithm would have high mAP.5 performance and short processing time, placing it in the upper-left region of the figure. As observed, DISPATCH outperforms all other baselines in terms of effectiveness, while maintaining reasonable efficiency. Although PAD achieves the second best result on mAP.5, its average processing time for each image exceeds one minute, falls behind all the other methods. DISPATCH completes the regeneration stage in 0.28 seconds and the rectification stage in 0.04 seconds per image. Although this is not the fastest, it remains within a practical range. DISPATCH strikes a balance between effectiveness and efficiency. This makes it particularly well-suited for offline processing applications where

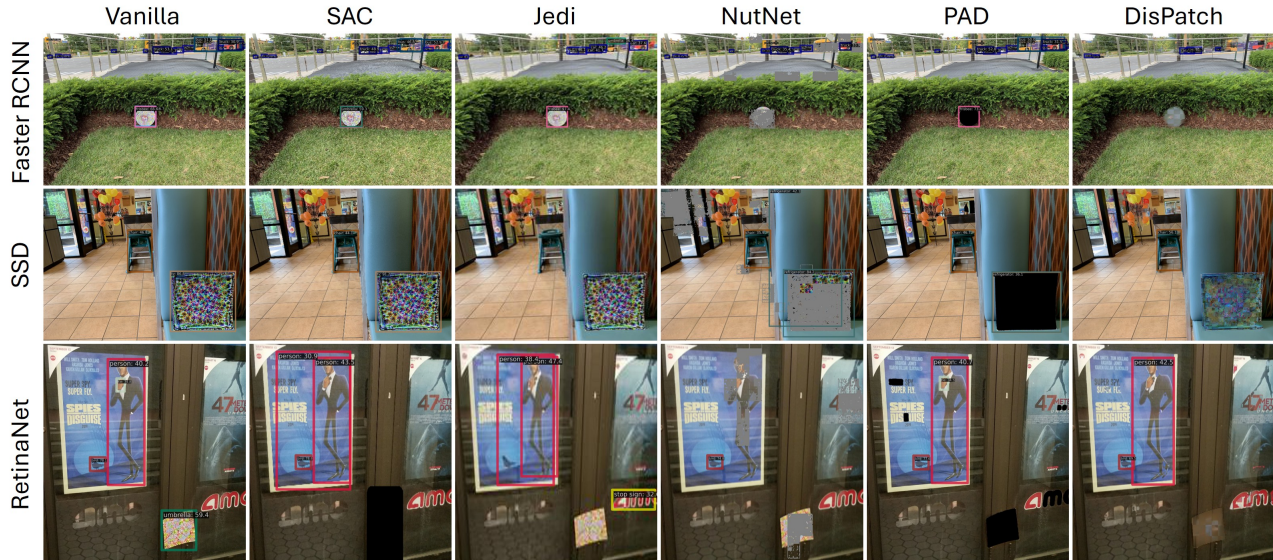


Figure 5: Qualitative results of our DISPATCH compared with the baseline methods when defending Faster RCNN, SSD, and RetinaNet on APRICOT dataset.

real-time constraints are relaxed, such as post-event surveillance video analysis, or batch processing in security systems. In such contexts, the slightly longer processing time is a worthwhile trade-off for the significantly enhanced detection performance and broader protection coverage against diverse attacks.

5.5. Robustness Analysis

An important aspect of an adversarial defense algorithm is its robustness against future adaptive attacks. Adaptive attacks refer to scenarios in which attackers adjust their strategy based on knowledge of the deployed defense mechanisms. In our setting, we assume that the attacker is aware of both the DISPATCH defense and the victim object detector, and thus constructs a new adversarial attack specifically designed to evade the defense.

To simulate an adaptive attack against the DISPATCH defense, the attacker can add an additional term to the loss function for optimizing the patch, alongside the original attack loss function:

$$\mathcal{L} = \mathcal{L}_{attack} + \alpha \mathcal{L}_{DISPATCH} \quad (8)$$

where \mathcal{L}_{attack} is the original attack loss function, $\mathcal{L}_{DISPATCH}$ is the loss function for evading DISPATCH, and α controls the importance of $\mathcal{L}_{DISPATCH}$. Since DISPATCH uses the L2 distance between the original input image I and the regenerated image \tilde{I} to identify adversarial regions, we define $\mathcal{L}_{DISPATCH}$ as the average pixel L2 distance between a patch δ and its regenerated counterpart $\tilde{\delta}$:

$$\mathcal{L}_{DISPATCH} = \mu(\|\delta - \tilde{\delta}\|_2) \quad (9)$$

where μ represents the average over all pixels within δ . In this way, we can force the adversarial patch to retain

its original pattern even after undergoing the diffusion regeneration stage, thereby increasing its chances of evading detection by Algorithm 1. We experiment with four different values of α : 0, 0.5, 1, and 5.0, to launch adaptive YOLOv3-AdvPatch attacks and YOLOv3-NatPatch attacks on INRIA-Person dataset, where $\alpha = 0$ corresponds to a non-adaptive attack baseline.

The results of adaptive attacks are shown in Table 4. For each adaptive attack, we report the mAP.5 performance of the victim object detector, without any defense (Vanilla) or with DISPATCH defense. As we can see from the table, non-adaptive AdvPatch attack and NatPatch attacks reduce the mAP.5 of vanilla YOLOv3 to 0.498 and 0.707, respectively. Adding $\mathcal{L}_{DISPATCH}$ to the loss function significantly weakens the attack capability of both AdvPatch and NatPatch attacks. When $\alpha = 0.5$, vanilla YOLOv3 obtains much better performance, with 0.761 under adaptive AdvPatch attack and 0.765 under adaptive NatPatch attack. As α increases, the attack capability continues to decline, since the optimization process shifts focus toward evading the defense rather than targeting the victim detector. However, these adaptive attacks still fail to evade the defense of DISPATCH. With DISPATCH applied, the detection performance of the victim detector is restored, reaching mAP.5 scores higher than 90% under adaptive AdvPatch attack, and over 84% under adaptive NatPatch attack.

To further analyze the reason behind this phenomenon, we visualize the behavior of the two loss functions, $\mathcal{L}_{DISPATCH}$ and \mathcal{L}_{attack} , during the training of an adaptive AdvPatch attack. Figure 6 shows the loss values over iterations, along with the inner product of their gradients. As illustrated, it is hard to optimize these two losses $\mathcal{L}_{DISPATCH}$ and \mathcal{L}_{attack} at the same time, as they do not converge even after 5000 iterations. Moreover, the right subplot reveals that

TABLE 4: mAP.5 results of YOLOv3 on INRIA-Person under different adaptive attacks, where $\alpha = 0$ means non-adaptive attack.

Attacks	Defense	$\alpha = 0$	$\alpha = 0.5$	$\alpha = 1.0$	$\alpha = 5.0$
AdvPatch	Vanilla	0.498	0.761	0.802	0.857
	DISPATCH	0.903	0.908	0.908	0.904
NatPatch	Vanilla	0.707	0.765	0.808	0.826
	DISPATCH	0.840	0.845	0.864	0.868

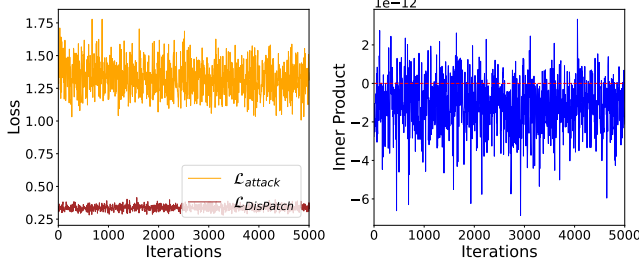


Figure 6: Left: losses over iterations of $\mathcal{L}_{DisPatch}$ and \mathcal{L}_{attack} . Right: the inner product of their gradients over iterations.

the inner product between their gradients remains negative throughout almost all iterations, indicating that *their optimization directions are largely contradictory*. This finding aligns with the observation from NutNet [24], and explains why these two losses do not converge over iterations. We show some examples of adaptive YOLOv3-NatPatch attacked images and their corresponding adversarial masks \mathcal{A} detected by DISPATCH in Figure 7. As the value of α increases, the adaptive attacks become more effective at evading DISPATCH, where fewer adversarial regions are detected. However, this comes at the cost of reduced attack strength, as shown in Table 4. Despite these evasions in some cases, the overall performance of DISPATCH maintains stable, demonstrating its robustness against adaptive adversarial attacks.

6. Discussion

Computational latency. The main limitation of DISPATCH lies in its time complexity, with an average processing time of 0.32 seconds per image. While this may pose challenges for time-critical applications, such as autonomous driving, it is well-suited for offline or near real-time scenarios like surveillance video analysis, forensic review, or batch processing in security pipelines. Importantly, this modest computational cost brings substantial gains in robustness and defense effectiveness. Furthermore, DISPATCH offers clear opportunities for future optimization, such as adopting lightweight diffusion architectures, model pruning, or quantization, paving the way for broader deployment across various operational settings.

Alternative generative models. DISPATCH leverages diffusion models for in-distribution reconstruction, but can other generative models be used? To investigate, we replaced LDM with a Masked Autoencoder (MAE) [48] in a small-

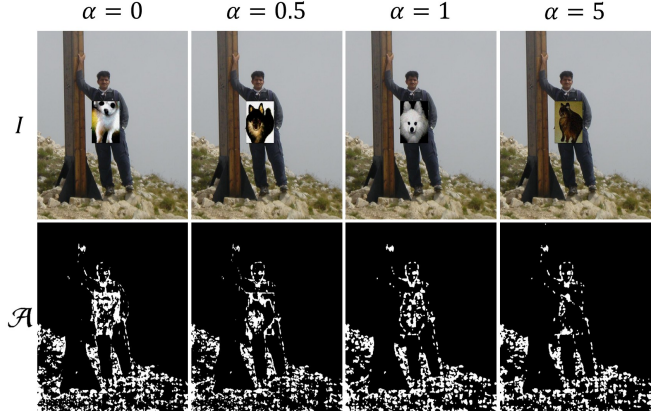


Figure 7: Qualitative results of adaptive YOLOv3-NatPatch attacks with different α . Top row: attacked images, bottom row: adversarial masks detected by DISPATCH.

scale experiment on INRIA-Person with YOLOv3 detector. The MAE-based variant showed only a minor drop of 1% in mAP.5 and 2% in AR, likely due to lower reconstruction quality of MAE. These results highlight the adaptability of DISPATCH, suggesting its potential to benefit from future advances in generative modeling.

Other potential risks. Our threat model assumes that the adversary has full knowledge of the architecture and weights of both the victim detector and the defense method, but lacks the capability to tamper with or modify them. This assumption can be reasonably upheld by using models trained in-house or obtained from trusted sources. However, incorporating models or training data from untrusted sources introduces the risk of backdoor attacks [49]. For instance, if the diffusion model in DISPATCH is compromised via a backdoor, an attacker could exploit hidden triggers to manipulate the generated image, potentially rendering the defense ineffective. Although such scenarios fall outside the scope of our current threat model, we acknowledge their significance and leave the exploration of backdoor-resistant scenarios for future work.

7. Conclusion

In this paper, we proposed DISPATCH, a novel diffusion-based defense method to defend object detectors against both hiding and creating adversarial patch attacks. By implementing a two-stage pipeline, namely (i) regeneration with inpainting diffusion models and (ii) rectification through an adversarial detection algorithm, DISPATCH effectively neutralizes malicious patches without any prior knowledge thereof. Our evaluations on two benchmarks and real-world scenarios demonstrate that DISPATCH consistently outperforms SOTA defense methods across different detectors and attacks, and is resilient against adaptive attacks. We hope that generative model-based defenses such as DISPATCH will contribute to advancing the security and robustness of object detection systems.

References

- [1] D. K. Jain, X. Zhao, C. Gan, P. K. Shukla, A. Jain, and S. Sharma, "Fusion-driven deep feature network for enhanced object detection and tracking in video surveillance systems," *Information Fusion*, vol. 109, p. 102429, 2024.
- [2] S.-D. Achirei, R. Mocanu, A.-T. Popovici, and C.-C. Dosofoi, "Model-predictive control for omnidirectional mobile robots in logistic environments based on object detection using cnns," *Sensors*, vol. 23, no. 11, p. 4992, 2023.
- [3] K. Muhammad, A. Ullah, J. Lloret, J. Del Ser, and V. H. C. de Albuquerque, "Deep learning for safe autonomous driving: Current challenges and future directions," *IEEE Transactions on Intelligent Transportation Systems*, vol. 22, no. 7, pp. 4316–4336, 2020.
- [4] Y. Ghasemi, H. Jeong, S. H. Choi, K.-B. Park, and J. Y. Lee, "Deep learning-based object detection in augmented reality: A systematic review," *Computers in Industry*, vol. 139, p. 103661, 2022.
- [5] J. Redmon, "Yolov3: An incremental improvement," *arXiv preprint arXiv:1804.02767*, 2018.
- [6] S. Ren, K. He, R. Girshick, and J. Sun, "Faster r-cnn: Towards real-time object detection with region proposal networks," *IEEE transactions on pattern analysis and machine intelligence*, vol. 39, no. 6, pp. 1137–1149, 2016.
- [7] N. Carion, F. Massa, G. Synnaeve, N. Usunier, A. Kirillov, and S. Zagoruyko, "End-to-end object detection with transformers," in *European conference on computer vision*. Springer, 2020, pp. 213–229.
- [8] A. Sharma, Y. Bian, P. Munz, and A. Narayan, "Adversarial patch attacks and defences in vision-based tasks: A survey," *arXiv preprint arXiv:2206.08304*, 2022.
- [9] A. Guesmi, M. A. Hanif, B. Ouni, and M. Shafique, "Physical adversarial attacks for camera-based smart systems: Current trends, categorization, applications, research challenges, and future outlook," *IEEE Access*, 2023.
- [10] A. Kurakin, I. J. Goodfellow, and S. Bengio, "Adversarial examples in the physical world," in *Artificial intelligence safety and security*. Chapman and Hall/CRC, 2018, pp. 99–112.
- [11] K. Eykholt, I. Evtimov, E. Fernandes, B. Li, A. Rahmati, C. Xiao, A. Prakash, T. Kohno, and D. Song, "Robust physical-world attacks on deep learning visual classification," in *Proceedings of the IEEE conference on computer vision and pattern recognition*, 2018, pp. 1625–1634.
- [12] S. Thys, W. Van Ranst, and T. Goedemé, "Fooling automated surveillance cameras: adversarial patches to attack person detection," in *Proceedings of the IEEE/CVF conference on computer vision and pattern recognition workshops*, 2019, pp. 0–0.
- [13] Y.-C.-T. Hu, B.-H. Kung, D. S. Tan, J.-C. Chen, K.-L. Hua, and W.-H. Cheng, "Naturalistic physical adversarial patch for object detectors," in *Proceedings of the IEEE/CVF International Conference on Computer Vision*, 2021, pp. 7848–7857.
- [14] Z. Hu, S. Huang, X. Zhu, F. Sun, B. Zhang, and X. Hu, "Adversarial texture for fooling person detectors in the physical world," in *Proceedings of the IEEE/CVF conference on computer vision and pattern recognition*, 2022, pp. 13 307–13 316.
- [15] Z. Hu, W. Chu, X. Zhu, H. Zhang, B. Zhang, and X. Hu, "Physically realizable natural-looking clothing textures evade person detectors via 3d modeling," in *Proceedings of the IEEE/CVF Conference on Computer Vision and Pattern Recognition*, 2023, pp. 16 975–16 984.
- [16] Y. Cao, S. H. Bhupathiraju, P. Naghavi, T. Sugawara, Z. M. Mao, and S. Rampazzi, "You can't see me: Physical removal attacks on {lidar-based} autonomous vehicles driving frameworks," in *32nd USENIX Security Symposium (USENIX Security 23)*, 2023, pp. 2993–3010.
- [17] S. Liu, J. Wang, A. Liu, Y. Li, Y. Gao, X. Liu, and D. Tao, "Harnessing perceptual adversarial patches for crowd counting," in *Proceedings of the 2022 ACM SIGSAC conference on computer and communications security*, 2022, pp. 2055–2069.
- [18] M. Yin, S. Li, C. Song, M. S. Asif, A. K. Roy-Chowdhury, and S. V. Krishnamurthy, "Adc: Adversarial attacks against object detection that evade context consistency checks," in *Proceedings of the IEEE/CVF winter conference on applications of computer vision*, 2022, pp. 3278–3287.
- [19] W. Zhu, X. Ji, Y. Cheng, S. Zhang, and W. Xu, "{TPatch}: A triggered physical adversarial patch," in *32nd USENIX Security Symposium (USENIX Security 23)*, 2023, pp. 661–678.
- [20] M. Noppel and C. Wressnegger, "Sok: Explainable machine learning in adversarial environments," in *2024 IEEE Symposium on Security and Privacy (SP)*. IEEE, 2024, pp. 2441–2459.
- [21] C. Xiang and P. Mittal, "DetectorGuard: Provably securing object detectors against localized patch hiding attacks," in *Proceedings of the 2021 ACM SIGSAC Conference on Computer and Communications Security*, 2021, pp. 3177–3196.
- [22] J. Feng, J. Li, C. Miao, J. Huang, W. You, W. Shi, and B. Liang, "Fight fire with fire: Combating adversarial patch attacks using pattern-randomized defensive patches," in *2025 IEEE Symposium on Security and Privacy (SP)*. IEEE Computer Society, 2024, pp. 6–6.
- [23] C. Xiang, A. Valtchanov, S. Mahloujifar, and P. Mittal, "Objectseeker: Certifiably robust object detection against patch hiding attacks via patch-agnostic masking," in *2023 IEEE Symposium on Security and Privacy (SP)*. IEEE, 2023, pp. 1329–1347.
- [24] Z. Lin, Y. Zhao, K. Chen, and J. He, "I don't know you, but i can catch you: Real-time defense against diverse adversarial patches for object detectors," in *Proceedings of the 2024 ACM SIGSAC Conference on Computer and Communications Security*, 2024, pp. 3823–3837.
- [25] I. J. Goodfellow, J. Shlens, and C. Szegedy, "Explaining and harnessing adversarial examples," *arXiv preprint arXiv:1412.6572*, 2014.
- [26] E. D. Cubuk, B. Zoph, S. S. Schoenholz, and Q. V. Le, "Intriguing properties of adversarial examples," *arXiv preprint arXiv:1711.02846*, 2017.
- [27] R. Suvorov, E. Logacheva, A. Mashikhin, A. Remizova, A. Ashukha, A. Silvestrov, N. Kong, H. Goka, K. Park, and V. Lempitsky, "Resolution-robust large mask inpainting with fourier convolutions," in *Proceedings of the IEEE/CVF winter conference on applications of computer vision*, 2022, pp. 2149–2159.
- [28] R. Rombach, A. Blattmann, D. Lorenz, P. Esser, and B. Ommer, "High-resolution image synthesis with latent diffusion models," in *Proceedings of the IEEE/CVF conference on computer vision and pattern recognition*, 2022, pp. 10 684–10 695.
- [29] Y. Zhao, H. Zhu, R. Liang, Q. Shen, S. Zhang, and K. Chen, "Seeing isn't believing: Towards more robust adversarial attack against real world object detectors," in *Proceedings of the 2019 ACM SIGSAC conference on computer and communications security*, 2019, pp. 1989–2004.
- [30] A. Brauneig, A. Chakraborty, M. Krumdick, N. Lape, S. Leary, K. Manville, E. Merkhofer, L. Strickhart, and M. Walmer, "Apricot: A dataset of physical adversarial attacks on object detection," in *Computer Vision—ECCV 2020: 16th European Conference, Glasgow, UK, August 23–28, 2020, Proceedings, Part XXI 16*. Springer, 2020, pp. 35–50.
- [31] L. Huang, C. Gao, Y. Zhou, C. Xie, A. L. Yuille, C. Zou, and N. Liu, "Universal physical camouflage attacks on object detectors," in *Proceedings of the IEEE/CVF conference on computer vision and pattern recognition*, 2020, pp. 720–729.
- [32] J. Liu, A. Levine, C. P. Lau, R. Chellappa, and S. Feizi, "Segment and complete: Defending object detectors against adversarial patch attacks with robust patch detection," in *Proceedings of the IEEE/CVF Conference on Computer Vision and Pattern Recognition*, 2022, pp. 14 973–14 982.

- [33] B. Tarchoun, A. Ben Khalifa, M. A. Mahjoub, N. Abu-Ghazaleh, and I. Alouani, “Jedi: Entropy-based localization and removal of adversarial patches,” in *Proceedings of the IEEE/CVF Conference on Computer Vision and Pattern Recognition*, 2023, pp. 4087–4095.
- [34] L. Jing, R. Wang, W. Ren, X. Dong, and C. Zou, “Pad: Patch-agnostic defense against adversarial patch attacks,” in *Proceedings of the IEEE/CVF Conference on Computer Vision and Pattern Recognition*, 2024, pp. 24 472–24 481.
- [35] Z. Chang, G. A. Koulteris, and H. P. Shum, “On the design fundamentals of diffusion models: A survey,” *arXiv preprint arXiv:2306.04542*, 2023.
- [36] J. Ho, A. Jain, and P. Abbeel, “Denoising diffusion probabilistic models,” *Advances in neural information processing systems*, vol. 33, pp. 6840–6851, 2020.
- [37] C. Saharia, J. Ho, W. Chan, T. Salimans, D. J. Fleet, and M. Norouzi, “Image super-resolution via iterative refinement,” *IEEE transactions on pattern analysis and machine intelligence*, vol. 45, no. 4, pp. 4713–4726, 2022.
- [38] J. Song, C. Meng, and S. Ermon, “Denoising diffusion implicit models,” *arXiv preprint arXiv:2010.02502*, 2020.
- [39] W. Nie, B. Guo, Y. Huang, C. Xiao, A. Vahdat, and A. Anandkumar, “Diffusion models for adversarial purification,” in *International Conference on Machine Learning*. PMLR, 2022, pp. 16 805–16 827.
- [40] Z. Liu, J. P. Zhou, Y. Wang, and K. Q. Weinberger, “Unsupervised out-of-distribution detection with diffusion inpainting,” in *International Conference on Machine Learning*. PMLR, 2023, pp. 22 528–22 538.
- [41] J. MacQueen *et al.*, “Some methods for classification and analysis of multivariate observations,” in *Proceedings of the fifth Berkeley symposium on mathematical statistics and probability*, vol. 1, no. 14. Oakland, CA, USA, 1967, pp. 281–297.
- [42] T.-Y. Lin, M. Maire, S. Belongie, J. Hays, P. Perona, D. Ramanan, P. Dollár, and C. L. Zitnick, “Microsoft coco: Common objects in context,” in *Computer Vision—ECCV 2014: 13th European Conference, Zurich, Switzerland, September 6–12, 2014, Proceedings, Part V 13*. Springer, 2014, pp. 740–755.
- [43] N. Dalal and B. Triggs, “Histograms of oriented gradients for human detection,” in *2005 IEEE computer society conference on computer vision and pattern recognition (CVPR’05)*, vol. 1. Ieee, 2005, pp. 886–893.
- [44] K. Chen, J. Wang, J. Pang, Y. Cao, Y. Xiong, X. Li, S. Sun, W. Feng, Z. Liu, J. Xu, Z. Zhang, D. Cheng, C. Zhu, T. Cheng, Q. Zhao, B. Li, X. Lu, R. Zhu, Y. Wu, J. Dai, J. Wang, J. Shi, W. Ouyang, C. C. Loy, and D. Lin, “MMDetection: Open mmlab detection toolbox and benchmark,” *arXiv preprint arXiv:1906.07155*, 2019.
- [45] EAVISE, “adversarial-yolo,” <https://gitlab.com/EAVISE/adversarial-yolo>.
- [46] W. Liu, D. Anguelov, D. Erhan, C. Szegedy, S. Reed, C.-Y. Fu, and A. C. Berg, “Ssd: Single shot multibox detector,” in *Computer Vision—ECCV 2016: 14th European Conference, Amsterdam, The Netherlands, October 11–14, 2016, Proceedings, Part I 14*. Springer, 2016, pp. 21–37.
- [47] T.-Y. Ross and G. Dollár, “Focal loss for dense object detection,” in *proceedings of the IEEE conference on computer vision and pattern recognition*, 2017, pp. 2980–2988.
- [48] K. He, X. Chen, S. Xie, Y. Li, P. Dollár, and R. Girshick, “Masked autoencoders are scalable vision learners,” in *Proceedings of the IEEE/CVF conference on computer vision and pattern recognition*, 2022, pp. 16 000–16 009.
- [49] Y. Li, Y. Jiang, Z. Li, and S.-T. Xia, “Backdoor learning: A survey,” *IEEE transactions on neural networks and learning systems*, vol. 35, no. 1, pp. 5–22, 2022.

Appendix A. Ablation Study

A.1. The Benefit of Rectification Process

Ideally, the regenerated image \tilde{I} should represent an in-distribution counterpart for the input image I , and should be suitable for further detection. However, the regeneration process is not always reliable and may affect benign objects. We present the performance of DISPATCH defending YOLOv3 against hiding attacks on INRIA-Person, with and without the rectification process, in Table 5. As observed from the table, when directly using the regenerated image for further object detection, the defense performance is significantly worse, as the regeneration process may affect the original objects. After adding the rectification process, the performance of victim detector improves a lot, showing that our rectification stage can help preserve benign data and eliminate adversarial effects at the same time. We expect that, in the future, more advanced diffusion models will achieve better defense performance with a single regeneration process, without impacting the quality of original images.

TABLE 5: The performance of DISPATCH for YOLOv3 without (W/O) or with (W/) the rectification process on INRIA-Person dataset.

Metric	mAP.5			
	Clean	AdvPatch	NatPatch	AdvTexture
W/O	0.928	0.853	0.776	0.807
W/	0.934	0.903	0.840	0.873

A.2. Adversarial Detection Algorithm

We show some examples of the original input images I , predicted adversarial masks \mathcal{A} by Algorithm 1, and the final output images \hat{I} of DISPATCH in Figure 8, including a clean image and several attacked images targeting Faster RCNN. As seen in the figure, for clean images, only some edges are detected as the adversarial mask. In the case of different patch attacks, Algorithm 1 can successfully identify adversarial patches and replace them with regenerated benign counterparts, thereby mitigating their impact. Although some benign regions may be included in the mask \mathcal{A} , they won’t be directly removed, but will instead be replaced with similar content generated by DISPATCH. Thus, the semantic integrity of the original image is preserved. To evaluate the accuracy of the proposed adversarial detection algorithm, we replace the identified adversarial regions with gray pixels, as done in NutNet [24], and denote this variant as DISPATCH(G). In this case, Eq. 7 becomes $\hat{I} = \mathcal{A} \odot I_{gray} \oplus (1 - \mathcal{A}) \odot I$, where I_{gray} is a gray image. The defense results of DISPATCH(G) on the INRIA-Person dataset, compared to NutNet, are shown in Table 6. DISPATCH(G) performs slightly worse than NutNet on clean images, but obtains in general better or similar performance when facing different attacks, with the only exception of

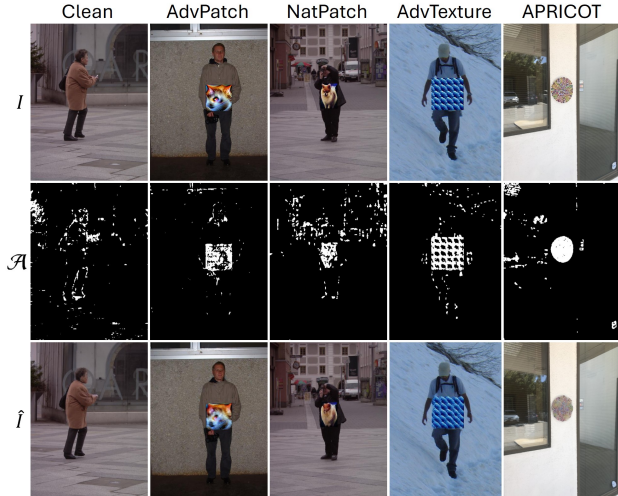


Figure 8: Input images I , regenerated images \tilde{I} , and predicted adversarial masks \mathcal{A} for different attacks on Faster RCNN.

TABLE 6: mAP.5 performance of DISPATCH(G) on INRIA-Person dataset comparing with NutNet and default DISPATCH.

Detector	metric	NutNet	DISPATCH(G)	DISPATCH
YOLOv3	Clean	0.919	0.909	0.934
	AdvPatch	0.808	0.897	0.903
	NatPatch	0.746	0.780	0.840
	AdvTexture	0.811	0.799	0.873
Faster RCNN	Clean	0.960	0.936	0.965
	AdvPatch	0.852	0.872	0.932
	NatPatch	0.750	0.846	0.906
	AdvTexture	0.686	0.791	0.814
DETR	Clean	0.949	0.928	0.954
	AdvPatch	0.861	0.873	0.932
	NatPatch	0.899	0.859	0.925
	AdvTexture	0.897	0.785	0.909

DETR-AdvTexture. When defending Faster RCNN, DISPATCH(G) significantly outperforms NutNet. These results demonstrate that Algorithm 1 is a simple yet effective approach for identifying the potential adversarial patches. Moreover, DISPATCH significantly improves the performance of DISPATCH(G), showing that our rectification approach works better than the traditional removal approach.

A.3. Number of Grids N

As all the input images are resized to 512×512 for processing in DISPATCH, the number of grids N directly determines the grid size in the checkerboard masks. We change the values of N and report the mAP.5 performance of DISPATCH for different hiding attacks on INRIA-Person in Table 7. As we can see from the table, compared to the default $N = 32$, the smaller value of $N = 16$ generally leads to performance degradation of at most 5%. This degradation occurs because a smaller N results in larger grid sizes in the inpainting masks during the regeneration stage. Some masked grids may cover small objects, causing the inpaint-

TABLE 7: The impact of N on DISPATCH performance (mAP.5) on INRIA-Person dataset.

Detector	N	16	32	64
YOLOv3	Clean	0.929	0.934	0.875
	AdvPatch	0.888	0.903	0.747
	NatPatch	0.822	0.840	0.646
	AdvTexture	0.823	0.873	0.734
Faster RCNN	Clean	0.950	0.965	0.885
	AdvPatch	0.914	0.932	0.751
	NatPatch	0.890	0.906	0.702
	AdvTexture	0.767	0.814	0.580
DETR	Clean	0.945	0.954	0.850
	AdvPatch	0.904	0.932	0.756
	NatPatch	0.911	0.925	0.754
	AdvTexture	0.863	0.909	0.764

TABLE 8: The time complexity and mAP.5 performance of DISPATCH with different diffusion sampling steps s , defending YOLOv3 on INRIA-Person dataset.

Sampling steps s		5	10	30	50
Time (seconds/img)		0.32	0.67	1.95	3.16
YOLOv3	Clean	0.934	0.929	0.934	0.934
	AdvPatch	0.903	0.896	0.899	0.901

ing method to inadvertently remove these objects. A larger $N = 64$ leads to much worse performance of DISPATCH, because it makes the grid size too small to provide sufficient context information during the regeneration stage. We observed that $N = 32$ is the optimal choice for handling different scenarios.

A.4. Sampling Steps s

The number of sampling steps s in diffusion models plays a crucial role in balancing output quality and computational efficiency. Generally, increasing s leads to higher quality image generation, but incurs greater inference time, whereas reducing s accelerates processing, making the model more suitable for real-time applications. In DISPATCH, we use a default setting of $s = 5$ to prioritize efficiency. To further understand this trade-off, we evaluate the performance of DISPATCH under varying sampling steps using both clean images and YOLOv3-AdvPatch attacked images, as shown in Table 8. Interestingly, we observe that increasing the number of sampling steps does not lead to better performance. We hypothesize that with fewer sampling steps, the regenerated image exhibits greater divergence from adversarial regions, which in turn enhances the contrast between benign and perturbed areas. Some visual examples with different sampling steps are shown in Figure 9. As illustrated in the figure, increasing the number of sampling steps enhances the preservation of details in the generated image \tilde{I} . For instance, the legs of the person on the right become more discernible. However, this improvement comes at the cost of increased inference time. In conclusion, the small value of $s = 5$ is the optimal choice for DISPATCH.



Figure 9: The generated image \tilde{I} and DISPATCH output image \hat{I} with different sampling steps s . Smaller sampling steps cause low quality in the generated image \tilde{I} , such as the legs of the person on the right. But the quality of final output will not be affected too much.

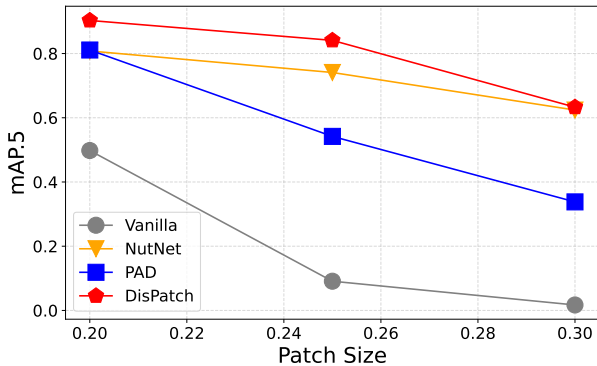


Figure 10: The impact of patch size on the performance of different defense methods against YOLOv3-AdvPatch attack.

A.5. Adversarial Patch Size

The default patch size scale ratio, defined as the ratio of the patch height to the diagonal length of the object bounding box, is set to 0.2 for AdvPatch and NatPatch, and 0.25 for AdvTexture. To evaluate the defense performance of the proposed DISPATCH on different sizes of adversarial patches, we modify the patch size scale ratio for the YOLOv3-AdvPatch attack and compare it with two baselines, NutNet and PAD. The results are shown in Figure 10. As observed, the mAP.5 performance of vanilla YOLOv3 drops rapidly as the adversarial patch size increases, resulting in less than 10% when the patch size is 0.3. PAD is sensitive to changes in patch size, it performs better than NutNet at the scale of 0.2, but becomes less effective as the patch size increases. Both NutNet and DISPATCH show their robustness against an increase in patch size, keeping mAP.5 score above 60% even when patch size is 0.3. Specifically, DISPATCH continuously outperforms NutNet on different patch sizes, demonstrating its stable defense capability.

Appendix B. Qualitative Examples

B.1. Qualitative Results of Defending Hiding Attacks on Faster-RCNN and DETR

We present qualitative comparisons of various defense methods for mitigating hiding attacks against Faster R-CNN and DETR in Figure 12 and Figure 13, respectively. For the Faster R-CNN results shown in Figure 12, adversarial examples generated using AdvPatch and AdvTexture successfully obscure parts of the human body. SAC performs well on AdvPatch and NatPatch, but only finds partial patch in AdvTexture. Jedi successfully located AdvPatch and NatPatch, but suffers from bad image quality. NutNet does not work on AdvTexture example, and PAD removes some benign regions on NatPatch example. The proposed DISPATCH effectively mitigates the effects of all three types of adversarial patches. For the DETR results illustrated in Figure 13, AdvPatch successfully hides the person, while NatPatch and AdvTexture introduce non-existent objects with the patches. SAC only works for AdvPatch, whereas Jedi fails to correct predictions in the AdvPatch example. NutNet and PAD both remove some benign regions and cannot solve the false positives. The proposed DISPATCH effectively mitigates the effects of all adversarial patches without introducing errors.

B.2. Qualitative Results on Real World Dataset

Figure 11 presents qualitative results of DISPATCH on our real-world dataset across various environmental conditions, including indoor settings, outdoor lighting (Outdoor-L), and outdoor shadows (Outdoor-S). As illustrated, DISPATCH effectively restores individuals hidden by adversarial patches in diverse scenarios, demonstrating its practical applicability in real-world environments.



Figure 11: Example results on real world dataset. DISPATCH successfully restores the person hidden by the patch, regardless of the environmental conditions.

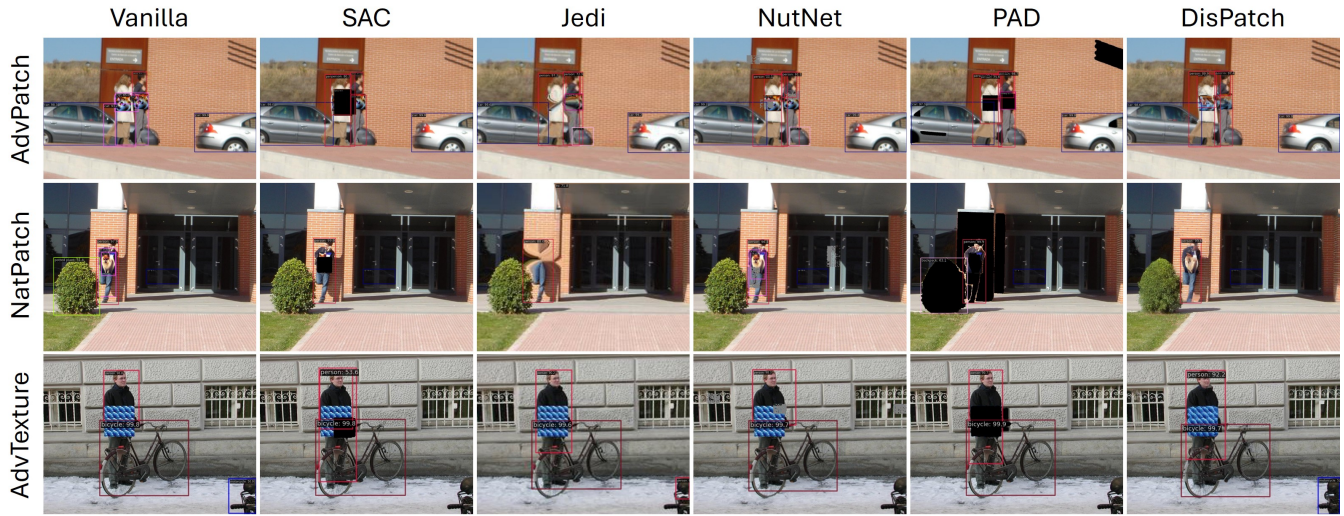


Figure 12: Qualitative results of our DISPATCH compared with the baseline methods when defending Faster RCNN against AdvPatch, NatPatch, and AdvTexture attacks on INRIA-Person dataset. Our DISPATCH can successfully restore the correct predictions in all three examples.

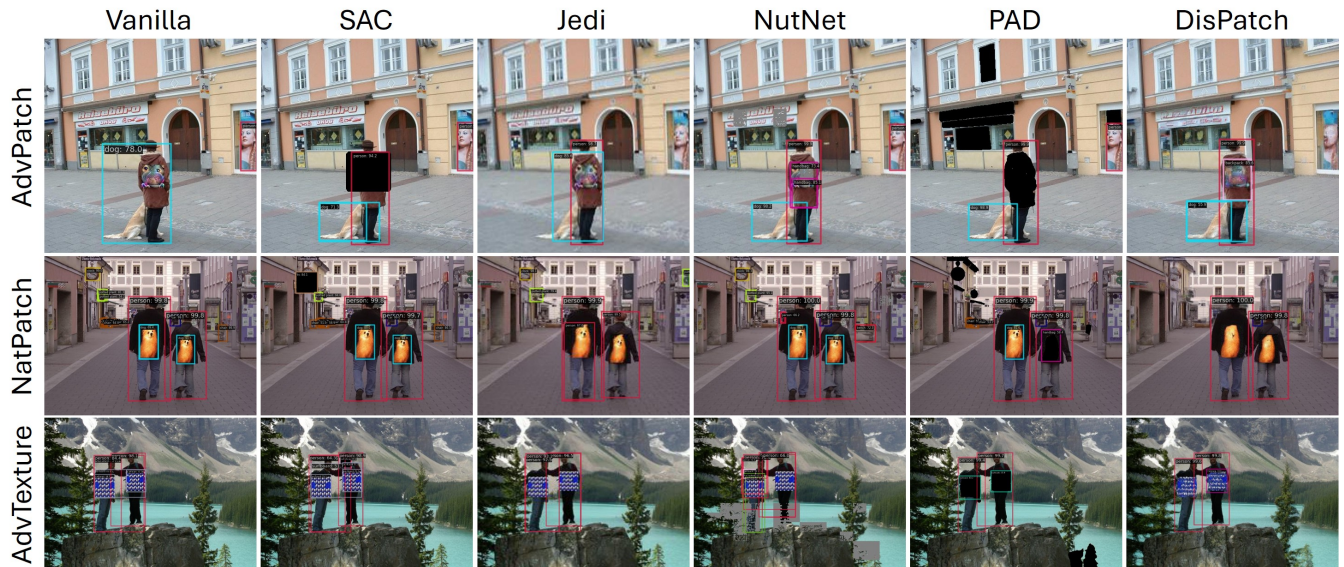


Figure 13: Qualitative results of our DISPATCH compared with the baseline methods when defending DETR against AdvPatch, NatPatch, and AdvTexture attacks on INRIA-Person dataset.